Functionalization of a Nano-Faujasite Zeolite with PEG-Grafted PMA Tethers Using Atom Transfer Radical Polymerization

Bi-Zeng Zhan, Mary Anne White,* Paul Fancy, Catherine A. Kennedy, and Michael Lumsden

Department of Chemistry and Institute for Research in Materials, Dalhousie University, Halifax, Nova Scotia, Canada B3H 4J3

Received July 23, 2003; Revised Manuscript Received February 4, 2004

ABSTRACT: We report the controlled growth of poly(ethylene glycol) methyl ether grafted polymethacrylate (PEGPMA) on nanosized zeolite external surfaces using the atom transfer radical polymerization (ATRP) approach. As-synthesized amino-modified faujasite zeolite nanoparticles (40 nm) were reacted with 2-bromoisobutyryl bromide to covalently bond bromine onto the zeolitic surfaces. The bromine atoms then serve as initiators for ATRP, allowing growth of a variety of polymer tethers onto the nanozeolite surfaces. The PEGPMA polymer has a unique structure in which very flexible PEO oligomers are bonded to stiff polymethacrylate backbones. This structure makes it possible to synthesize nanohybrid materials with a fully amorphous polymer phase, a main requirement for conductivity of solid polymer electrolytes. Raman spectroscopy and ^{13}C solid-state NMR spectroscopy were used to characterize the as-synthesized samples. Furthermore, both Raman spectroscopy and polymer molecular weight determinations demonstrated the controlled growth of polymer chains in the ATRP synthesis. DSC experiments indicated that a fully amorphous polymer phase can be achieved by properly controlling the polymerization conditions. The morphology of the polymer phase in PEGPMA−nanoNaX composites is very stable. DSC cycling scans in the temperature range −150 to 100 °C did not induce crystallization of the amorphous polymer segments. TEM images demonstrate significant variation of the zeolite surface properties after modification with polymer tethers, indicating that very dense hybrid zeolite-based thin films or membranes could be achieved using simple solvent-cast spin-coating techniques.

Introduction

Since the discovery of ionic conductivity in alkali metal salt complexes of poly(ethylene oxide) (PEO) in 1973,[1] interest in polymer electrolytes for use in lithium and lithium ion batteries has grown enormously.[2−6] It is now established that ionic conductivity is associated with the alignment, organization, and mobility of the polymer segments.[7−9] The conductivity is low at ambient temperature for PEO-based electrolytes because PEO is a semicrystalline polymer with a melting and recrystallization temperature of 62 and 48 °C (our DSC results, 10 K min^{-1} scanning rate, M_n ca. 10^5), respectively. The polymer matrix becomes too stiff to conduct lithium cations efficiently at a temperature lower than the melting point. Considerable effort has been focused on inhibiting or even eliminating recrystallization of PEO at ambient and even subambient temperatures. Hybrid organic−inorganic nanocomposite materials, formed by addition of inorganic nanoparticles into PEO matrices, have been found to significantly suppress recrystallization of PEO, therefore increasing the cationic transport number and electrode−electrolyte interface stability and enhancing the conductivity and mechanical properties.[10−14] Furthermore, any Lewis acids in the inorganic components can increase the Li^+ cationic transference number through Lewis acid−base interaction.[13,14] An alternative approach to achieve amorphous PEO segments is to graft very flexible ethylene oxide oligomers onto stiff polymer backbones, but this still remains synthetically challenging.[2]

The controlled/living radical polymerization (CRP) approach has been widely used to synthesize nanohybrid composite materials with molecular control of compositions and structures, allowing materials with tailored structural, surface, and other properties.[15] For example, SiO_2 nanoparticles have been covalently attached to a variety of polymer and block copolymer tethers by the atom transfer radical polymerization (ATRP) approach.[16−20] Microporous zeolitic materials have several advantages compared with SiO_2, Al_2O_3, MgO, TiO_2, and other inorganic nanoparticles, namely well-defined pores/cages, tunable base/acid sites, molecular sieve, and ion exchange capabilities.[21] For example, each aluminum atom in the zeolitic framework provides a negative charge. The Li^+ cation, which can be ion-exchanged into the well-defined zeolitic cages for charge balance, could provide a contribution for the cationic transference number. Ionic conductivity of Li^+-exchanged zeolites has been observed under various conditions.[22−26] Furthermore, the Lewis acid sites of zeolitic frameworks could provide another contribution in increasing the Li^+ cationic transference number through Lewis acid−base interactions.[13,14] These unique properties make nanozeolites good candidates as inorganic components for hybrid nanocomposites, which have potential as solid polymer electrolytes for secondary lithium batteries. There have been no reports of nanozeolites as the inorganic component for hybrid organic−inorganic nanocomposites. Recently, we have developed an organic-additive-free hydrothermal crystallization method to synthesize faujasite zeolites with controllable particle sizes and surface properties.[27,28] These materials are the basis for novel oxidation catalysts.[29] The as-synthesized nanometer-sized faujasite zeolite, hereafter referred to as nanoNaX (40 nm), displays attractive features such as a very large external surface area and numerous silanol groups on its exter-

* Corresponding author: Tel (902) 494 3894; Fax (902) 494 8016; e-mail Mary.Anne.White@dal.ca.

10.1021/ma035062z CCC: $27.50
Published on Web 03/23/2004

nal surfaces. The latter can serve as functional sites for chemical modification to covalently bond with a wide variety of organic functional groups.[30] Such functionalization opens up new avenues for creation of novel zeolite-based hybrid organic−inorganic composite materials. Here, we extend our research to the synthesis of polymer-functionalized nanozeolite composite materials. Using the ATRP approach, crystalline nanoNaX zeolite can be covalently bonded with poly(ethylene glycol) methyl ether grafted polymethacrylate polymer tethers, in which flexible ethylene oxide oligomers are grafted onto stiff polymethacrylate backbones. Novel hybrid composite materials having the combined advantages of zeolites and the unique structures of polymer tethers can be achieved.

Experimental Section

Materials. Chemical reagents included the following: fumed silica (11 nm, Sigma), NaOH (Aldrich), $Al(OH)_3$ (McArthur Chemical), $NaAlO_2$ (Allied Chemical), NaCl (Aldrich); (3-aminopropyl)triethoxysilane (99%, Aldrich), triethylamine (99.5%, Aldrich), 2-bromoisobutyryl bromide (98%, Aldrich), poly(ethylene glycol) methyl ether methacrylate (PEGMA, average M_n ca. 475, Aldrich), CuBr (98%, Aldrich), 4,4′-dinonyl-2,2′-dipyridyl (dNbpy, 97%, Aldrich), THF (Aldrich), and ethanol (Aldrich). These were used without further purification. Acetonitrile (Aldrich) was dried with 3A zeolite before use.

Instrumentation. FT-Raman spectra were recorded on a Bruker IFS 100 spectrometer equipped with a CW Nd:YAG laser (1064 nm excitation) and a Ge detector cooled with liquid N_2. All Raman spectra were collected with 180° scattering geometry and 4 cm^{-1} spectral resolution. Typically, a laser power of 150−250 mW was used to irradiate a loosely packed powder sample held in an aluminum holder. Over 2000 scans needed to be averaged in order to reach a reproducible signal-to-noise ratio. High-resolution TEM images were taken on a FEI Tecnai-12 microscope operated at 80 kV. Differential scanning calorimetry (DSC) measurements were performed on a Perkin-Elmer Pyris 1 in the temperature range −150 to 100 °C with a scanning rate of 10 K/min. The system was calibrated with the solid−solid phase transition of dipentylammonium chloride.[31] Solid-state NMR spectra were run on a Bruker AMX-400 (9.4 T) NMR spectrometer operating at 100.6 MHz. $^1H/^{13}C$ solid-state cross-polarization/magic-angle-spinning (CP/MAS) NMR spectra were recorded using a 7 kHz spinning rate. A relaxation delay of 8 s, 7 ms contact time, and over 20 000 scan numbers were adopted. Polymer molecular weight was determined by size exclusion chromatography using a Waters 515 HPLC pump connected to three Waters 5 μm Styragel linear columns and a Waters 2414 refractive index detector. The column and detector temperatures were set to 40.0 and 35.0 °C, respectively. THF was used as elution solvent (flow rate = 1 mL/min), and narrow-dispersion linear polystyrene standards were use for calibration. Composite samples were decomposed with HF aqueous solution and then neutralized. Organic polymers were extracted with THF and chloroform.

Synthesis of NanoNaX Zeolites. NanoNaX zeolite (40 nm, Figure 4a) was synthesized using the method we reported recently.[27,28] Here, nanoNaX modified on the external surfaces with (3-aminopropyl)silyl organic function groups, denoted as amino-nanoNaX, was synthesized by directly reacting nanoNaX zeolite (dried at 120 °C for 24 h) with (3-aminopropyl)triethoxysilane in toluene solvent under reflux conditions (see ref 30 for synthesis details).

Synthesis of Br-NanoNaX. A suspension of 1.5 g of dried amino-nanoNaX (120 °C, 24 h) and 40 mL of dried acetonitrile, in a round-bottomed flask with a stir bar, was cooled in an ice−water bath for 2 h. Then 0.49 mL of triethylamine was added dropwise. The mixture was stirred for another 30 min in the ice−water bath, and then 0.44 mL of 2-bromoisobutyryl bromide was added. The amidation reaction was conducted at 0 °C for 4 h, followed by another 20 h at room temperature. After this, a white powder, separated from the solvent by centrifugation, was fully washed with saturated aqueous NaCl solution, water, and ethanol to remove any physically adsorbed species. The sample was dried at 80 °C for 24 h before further characterization. The concentration of 2-bromoisobutyrate on the zeolite was about 1.3 mmol g^{-1}.

Scheme 1. Synthetic Procedures for PEGPMA-Modified NanoNaX

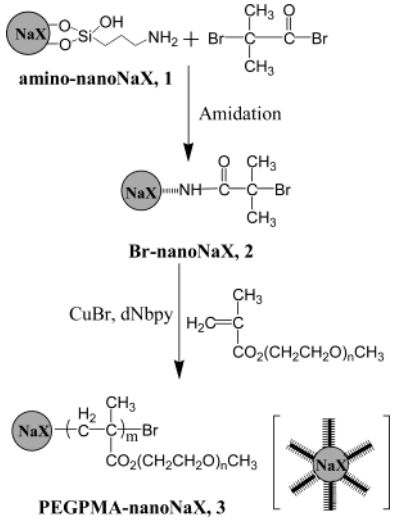

Growing PEGPMA Polymer Tethers onto NanoNaX. A mixture containing 0.2 g of Br-nanoNaX, 0.020 M CuBr, 0.040 M dNbpy (4,4′-dinonyl-2,2′-dipyridyl), and 2.3 M PEGMA (poly(ethylene glycol) methyl ether methacrylate monomer) was degassed with ultrahigh-purity N_2 for 2 h at room temperature. Atom transfer radical polymerization was conducted at 90 °C in a nitrogen atmosphere. The as-synthesized composites were fully washed with THF and then ethanol. All the samples were dried at 80 °C for 24 h before further characterization. Two samples, PEGPMA-nanoNaX (3.5 h) and PEGPMA-nanoNaX (10 h), were synthesized with different polymer tether lengths, where the value in the parentheses stands for the polymerization time.

Controlled Synthesis of PEGMA/NanoNaX. For comparison, a control sample was prepared by directly mixing PEGMA monomer and nanoNaX in ethanol solvent. The mixture was mixed and then heated to 80 °C to remove the solvent. The powder-like white material obtained is denoted as PEGMA/nanoNaX.

Results and Discussion

The synthetic procedures for the functionalization of nanoNaX zeolite are given in Scheme 1. The synthesis and characterization of (3-aminopropyl)silyl-modified nanoNaX (amino-nanoNaX, **1** in Scheme 1) have been reported elsewhere.[30] The 2-bromoisobutyrate groups, which served as initiators for atom transfer radical polymerization (ATRP), were grafted onto the surfaces of zeolite nanoparticles through amidation of amino-nanoNaX with 2-bromoisobutyryl bromide. The 2-bromoisobutyrate-modified sample obtained is denoted as Br-nanoNaX (**2** in Scheme 1). All the as-synthesized samples were characterized by Raman spectroscopy. Figure 1 gives the FT-Raman spectra of amino-nanoNaX and Br-nanoNaX along with pure nanoNaX. In comparison with amino-nanoNaX (Figure 1b), two new Raman peaks were found in Br-nanoNaX (Figure 1c). The new sharp peak at 1649 cm^{-1} is attributed to the C═O stretching mode of the amide in the 2-bromoisobutyrate groups, while the other strong peak at 298

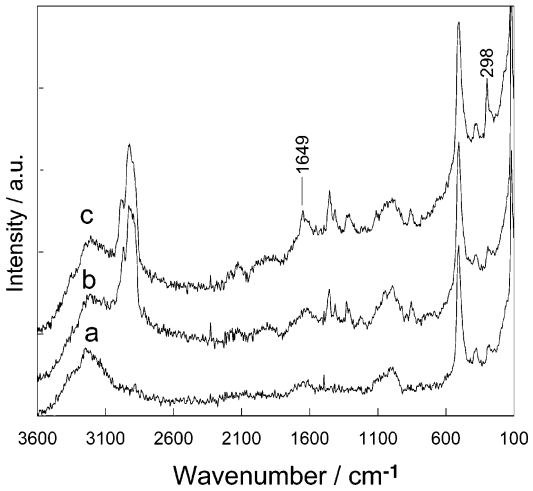

Figure 1. FT-Raman spectra of (a) nanoNaX, (b) amino-nanoNaX, and (c) Br-nanoNaX.

cm^{-1} is reasonably assigned to the C−Br stretching mode of 2-bromoisobutyrates.[32] The intensities of several other peaks, including C−H stretching modes at 2967 and 2915 cm^{-1} and C−H bends at 1400−1500 cm^{-1}, which overlap with the vibrations of the (3-aminopropyl)silyl groups covalently attached on the nanoNaX, are also enhanced after amidation. These results clearly indicate the success of transferring amino-nanoNaX to Br-nanoNaX.

The success of amidation is also confirmed by $^{1}H/^{13}C$ cross-polarization/magic angle spinning (CP/MAS) solid-state NMR spectroscopy. Figure 2 shows the CP/MAS spectra of amino-nanoNaX and Br-nanoNaX. The three ^{13}C resonances at 43, 22, and 11 ppm found in the amino-nanoNaX (Figure 2a) are attributed to the three carbons of the (3-aminopropyl)silyl groups, which have been fully discussed previously.[30] Amidation does not significantly change the chemical shifts of these three carbons. They are found at 42, 23, and 10 ppm, respectively, in the ^{13}C NMR spectrum of Br-nanoNaX (Figure 2b). Furthermore, three new carbon signals found at 172, 62, and 31 ppm in the ^{13}C NMR spectrum of Br-nanoNaX sample indicate the presence of the 2-bromoisobutyrate groups on the zeolite surfaces. The signal at 172 ppm is reasonably assigned to the carbon of the carbonyl group, while the ^{13}C signals at 62 and 31 ppm are attributed to the carbons directly connected to the Br atom and the two methyl groups, respectively. The full assignment of the Br-nanoNaX ^{13}C NMR spectrum is indicated in Figure 2.

The Br-nanoNaX particles, thus prepared, were then used as initiators to grow polymer tethers with monomers of poly(ethylene glycol) methyl ether methacrylate (PEGMA) using the ATRP approach. This method has been used to synthesize a poly(ethylene glycol) methyl ether methacrylate-based macromonomer using phenyl-2′-bromo-2′-methyl propionate as the initiator.[33] We have already demonstrated that Raman scattering techniques are powerful and sensitive in the studies of zeolite-based host−guest systems[34,35] and zeolite modified with organic functional groups.[30] Here, we show that FT-Raman spectroscopy is also a useful tool to verify the successful growth of polymer tethers by initiation from the external surfaces of zeolite nanoparticles. The Raman spectrum of poly(ethylene glycol) methyl ether grafted polymethacrylate−nanoNaX composite (**3** in Scheme 1), hereafter denoted as PEGPMA−

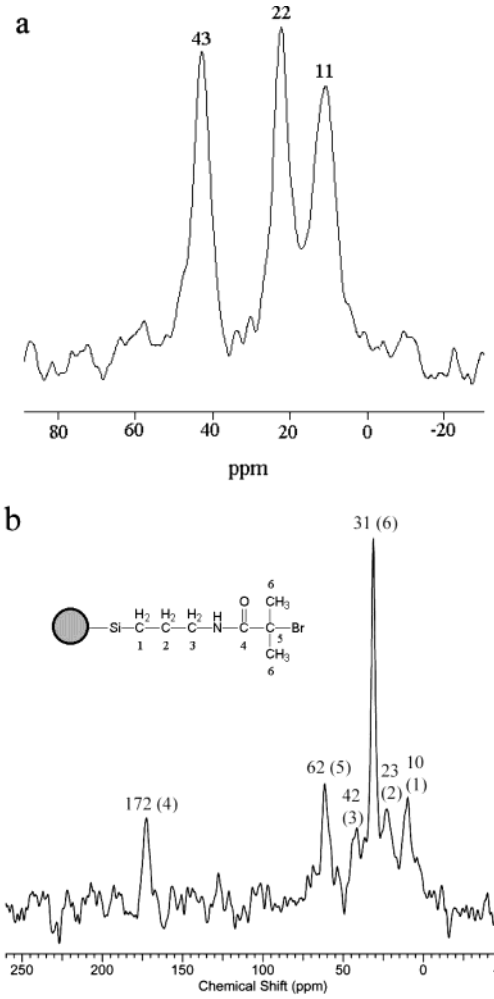

Figure 2. ^{13}C solid-state CP/MAS NMR spectra of (a) amino-nanoNaX and (b) Br-nanoNaX.

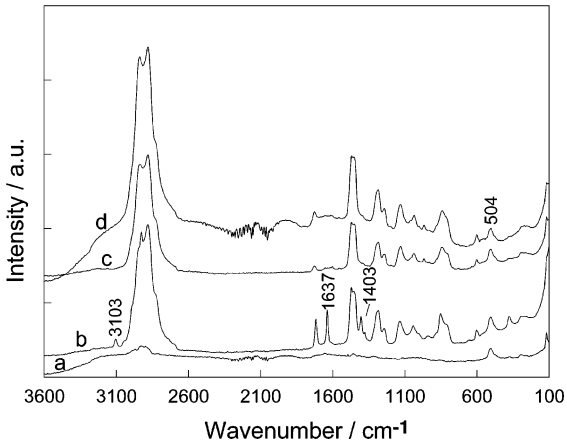

Figure 3. FT-Raman spectra of (a) "amino-nanoNaX", (b) PEGMA/nanoNaX, (c) PEGPMA−nanoNaX (3.5 h), and (d) PEGPMA−nanoNaX (10 h). For (a), amino-nanoNaX was used as "initiator" instead of Br-nanoNaX. All the synthetic conditions were exactly the same as those for PEGPMA−nanoNaX with 10 h for polymerization.

nanoNaX, is given in Figure 3 along with the Raman spectrum of a direct mixture of PEGMA monomer with nanoNaX (denoted as "PEGMA/nanoNaX", see Experimental Section for details) and that of a control sample (using amino-nanoNaX as "initiator"; see the caption to Figure 3 for details). Several vibrational features related to the methacrylate group of PEGMA monomer, such

Table 1. Molecular Masses of PEGPMA Polymer Tethers Grown on the External Zeolite Surfaces

polymerization time, h	3.5	10
M_n	4.9×10^4	7.1×10^4
M_w/M_n	4.7	4.1

as the C−H stretch at 3103 cm^{-1}, the C═C stretch at 1637 cm^{-1}, and the C−H bend at 1403 cm^{-1}, present in the PEGMA/nanoNaX (Figure 3b), have disappeared in the Raman spectra of PEGPMA−nanoNaX (Figure 3c,d). This provides evidence that the PEGPMA polymer was successfully attached to the zeolitic nanoparticles using the ATRP approach. Raman spectra of PEGPMA−nanoNaX samples suggest that no unpolymerized PEGMA monomer remains on the zeolite surface, indicating that the solvent washing method we adopted efficiently removes any physically adsorbed monomer. The presence of the characteristic T−O−T bend of the faujasite framework at 504 cm^{-1} in the Raman spectra of PEGPMA-nanoNaX composites clearly indicates that the zeolitic structure is retained after amidation and ATRP.[30,34,36] Furthermore, the length scale of polymer tethers can be tailored by controlling the polymerization time. This is reflected in the intensities of the Raman scattering peaks: with similar intensities for the characteristic zeolitic peaks at 504 cm^{-1}, the intensities of the peaks attributed to the organic polymer phase of PEGPMA−nanoNaX (after 10 h, Figure 3d) are much greater than that of PEGPMA−nanoNaX (after 3.5 h, Figure 3c). This finding concurs with the measurement of polymer molecular mass (Table 1). The number-averaged molecular weight (M_n) of the grafted polymer tethers, as determined by size-exclusion chromatography (SEC), increased with increased polymerization time from 4.9×10^4 in PEGPMA−nanoNaX (3.5 h) to 7.1×10^4 in PEGPMA−nanoNaX (10 h). The broad polydispersity (M_w/M_n, where M_w is weight-averaged molecular mass) and bimodal peaks (not shown) are attributed to polymer branching and broad dispersity of the monomer used.

The FT-Raman spectra indicate that no Raman signals belonging to monomer or polymer were found on the zeolitic surface when amino-nanoNaX was used as "initiator" instead of Br-nanoNaX in a control experiment (Figure 3a). This demonstrates that the polymer tethers only grow from the Br atom initiators attached to the external zeolite surface. It also indicates that unreacted PEGMA monomer can be completely removed through the solvent extraction process which we have adopted.

The surface properties of nanozeolites are significantly altered through the tethering of polymers. These changes were observed from the dispersion and stability of these zeolite-based nanohybrid materials in a variety of organic solvents and on various substrate surfaces. TEM images provide direct evidence. In contrast to the irregular arrangement of pure nanoNaX zeolite deposited on the TEM grid (Figure 4a), the nanocrystals of PEGPMA−nanoNaX (Figure 4b) conglomerate, forming a very dense thin film (about 100 nm thick as estimated from TEM images) on the TEM grid, likely due to strong interactions among the polymer tethers. These results imply the possibility of preparing thin hybrid zeolitic films or membranes using solvent-cast spin-coating techniques, which would be very useful in practical applications such as solid polymer electrolytes for secondary lithium batteries. Furthermore, in comparison with Figure 4a, the TEM image given in Figure 4c indicates that there is no change in the size of the zeolite particles during the ATRP processes.

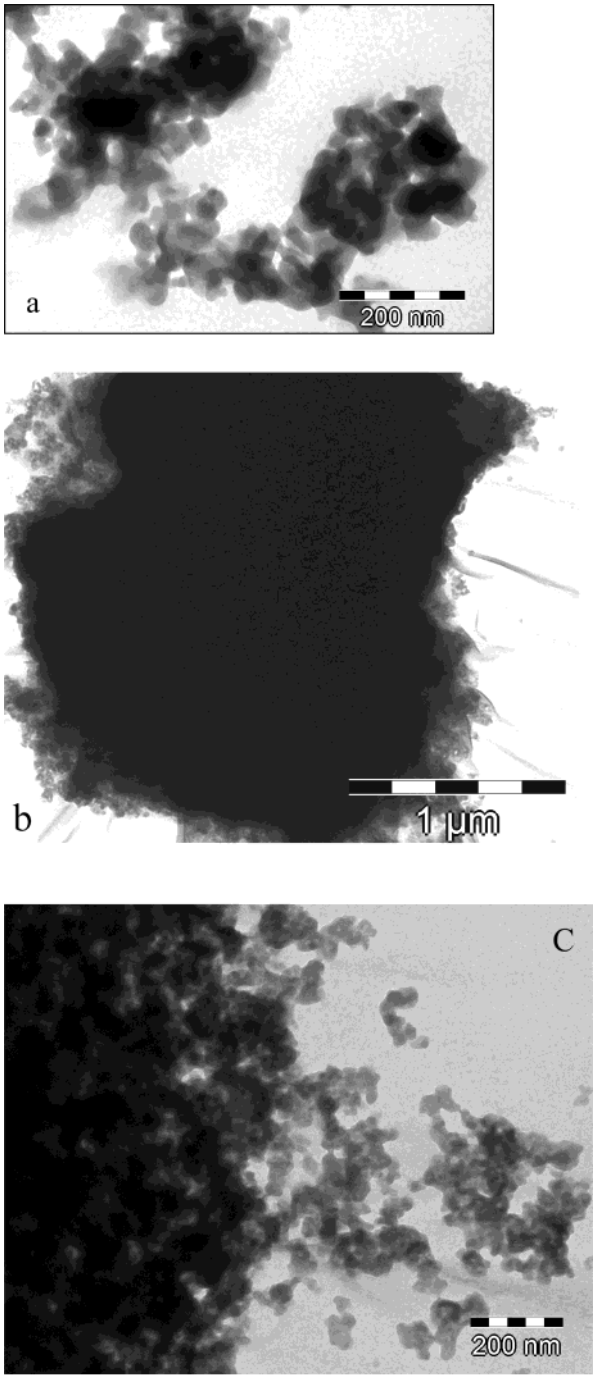

Figure 4. TEM images of (a) nanoNaX and (b, c) PEGPMA−nanoNaX (3.5 h).

Differential scanning calorimetry (DSC) was used to investigate the morphology of the organic polymer phases in the nanohybrid composites. DSC scans for hybrid polymer−nanozeolite composites are shown in Figure 5, along with the PEGMA monomer for comparison. The DSC results indicate that the PEGMA monomer has a broad melting process on heating and a sharp recrystallization process with an onset temperature of about −11 °C on cooling (Figure 5a). For the synthetic PEGPMA−nanoNaX composite material (10 h of polymerization), the melting process remained at a temperature similar to that of the monomer although reduced in enthalpy by about 90%, and recrystallization on cooling was significantly suppressed compared with the

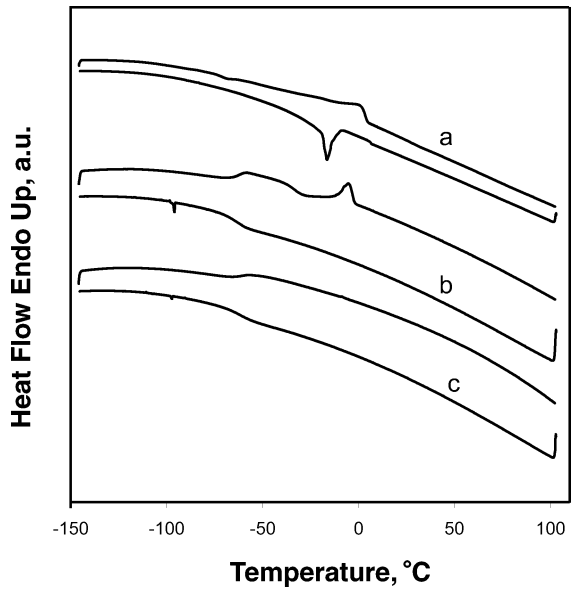

Figure 5. DSC scans for (a) PEGMA monomer, (b) PEGPMA−nanoNaX (10 h), and (c) PEGPMA−nanoNaX (3.5 h). In each case, the upper curve is on heating and the lower curve is on cooling. All the DSC scans started from heating. The sensitivity for (b) and (c) is about 10 times greater than for (a).

case of the monomer. This indicates that PEGPMA attached on the nanozeolite surface is partially crystallized, which is reasonable considering the semicrystalline properties of PEO-based polymers. Furthermore, a glass transition (T_g of −67 °C) was found (Figure 5b). The observation of this glass transition process provides further evidence for the successful growth of polymer tethers on the nanoNaX surfaces using the ATRP approach. Interestingly, Figure 5c indicates that both melting and recrystallization were eliminated in the sample prepared with a polymerization period of 3.5 h, demonstrating that the polymer phase attached on the zeolitic surface is completely amorphous. The glass transition temperatures are the same for the two PEGMA−nanoNaX composites synthesized with different polymerization periods. These results indicate that the organic polymer phase of PEGPMA can be fully amorphous at ambient or even subambient temperatures through molecular control of the synthesis. They further suggest the potential of PEGPMA−nanoNaX composite materials for high conductivity and utility as solid polymer electrolytes at ambient or even subambient temperatures.

Multicycle DSC experiments also were carried out to study the stability of the polymer phase in the as-synthesized PEGPMA−nanoNaX composites, and results are shown in Figure 6. The first three DCS scan cycles of PEGPMA−nanoNaX (3.5 h polymerization) composite (Figure 6a) indicate that cycling in the temperature range −150 to 100 °C did not induce recrystallization of the amorphous polymer phase. The degree of crystallization of the as-synthesized PEGPMA−nanoNaX sample with 10 h of polymerization, as estimated by the area of the peak centered at 0 °C, did not change during multiple DSC scans (Figure 6b). This shows the high thermal stability of PEGPMA−nanoNaX composites in a practical temperature range, which is important for stable solid polymer electrolytes. These PEGPMA−nanoNaX results contrast with observations of hybrid PEO−MgO composites made by directly mixing two components together, in which obvious changes

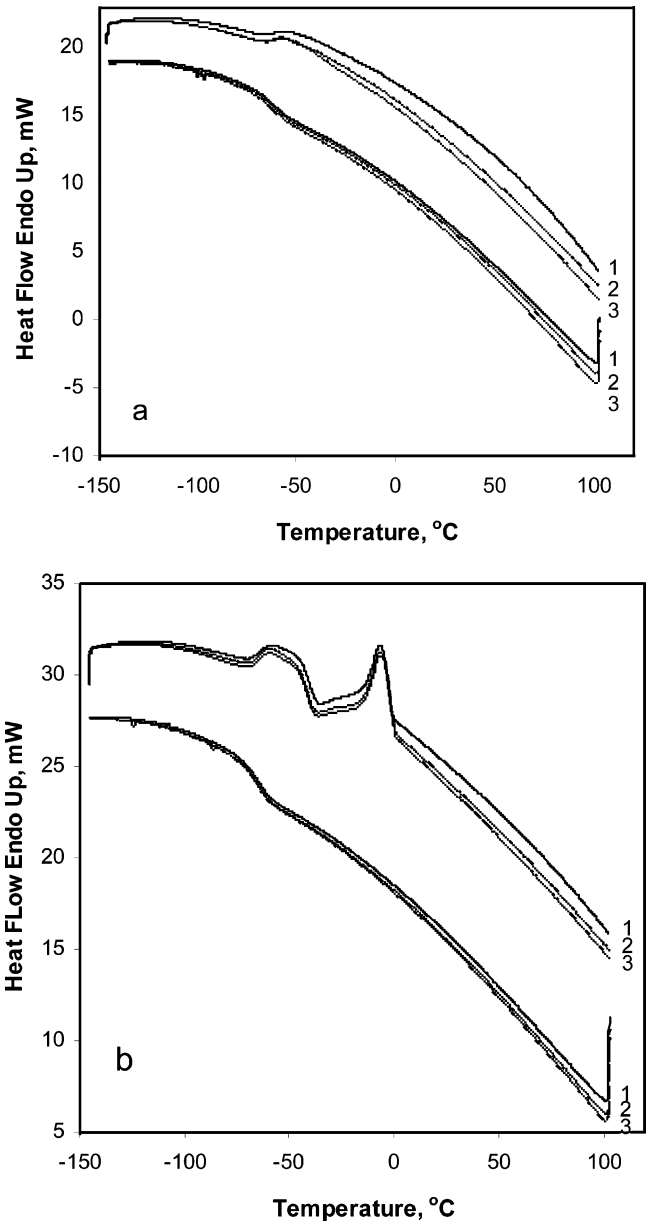

Figure 6. DSC cycling scans for PEGPMA−nanoNaX: (a) 3.5 h polymerization and (b) 10 h polymerization. In each case, the cycle numbers shown started from heating from −150 to 100 °C with a hold time of 0.5 h at −150 and 100 °C, respectively. The numbers represent the scan order. In each cycle, the upper curve is on heating and the lower curve is on cooling.

of polymer phase morphology were found in thermal cycling experiments.[12]

Conclusions

We have demonstrated that nanometer-sized faujasite zeolites can be covalently bonded with different length-scale poly(ethylene glycol) methyl ether grafted polymethacrylate tethers using an atom transfer radical polymerization approach. Raman and ^{13}C solid-state NMR spectroscopic techniques were employed to explore the presence and changes of the organic polymer phases in the nanozeolite-based hybrid composites. DSC results show that the organic polymer phases of PEGPMA−nanoNaX composites can be completely amorphous, with T_g of about −67 °C. DSC experiments also indicate that thermal cycling does not induce further

recrystallization of the amorphous polymer phases in the nanohybrid composites. In summary, the composite PEGPMA−nanoNaX has the following advanced characteristics: it is a hybrid PEO−inorganic composite with enhanced film-forming ability, stability, and mechanical properties; it can have completely amorphous polymer phases derived from molecularly controlled polymerization in which PEO oligomers are attached to stiff polymer backbones. These unique properties make these composites potentially useful as a novel solid polymer electrolyte for secondary lithium batteries.

Acknowledgment. This work was financially supported by the Natural Sciences and Engineering Research Council and the Killam Trusts (the latter for a research professorship to M.A.W., postdoctoral research fellowship to B.Z.Z., and scholarship to C.A.K.). We thank Professor H. Stover (McMaster University) for size-exclusion chromatography results and the Atlantic Region Magnetic Resonance Centre for NMR spectra.

References and Notes

(1) Fenton, D. E.; Parker, J. M.; Wright, P. V. *Polymer* **1973**, *14*, 589.
(2) Meyer, W. H. *Adv. Mater.* **1998**, *10*, 439.
(3) Armand, M. *Solid State Ionics* **1994**, *69*, 309.
(4) Tarascon, J.-M.; Armand, M. *Nature (London)* **2001**, *414*, 359.
(5) Wright, P. V. *MRS Bull.* **2002**, *27*, 597.
(6) Shriver, D. F.; Bruce, P. G. In *Solid State Electrochemistry*; Bruce, P. G., Ed.; Cambridge University Press: Cambridge, UK 1995.
(7) Gadjourova, Z.; Andreev, Y. G.; Tunstall, D. P.; Bruce, P. G. *Nature (London)* **2001**, *412*, 520.
(8) Zheng, Y.; Chia, F.; Ungar, G.; Wright, P. V. *Chem. Commun.* **2000**, 1459.
(9) Imrie, C. T.; Ingram, M. D.; McHattie, G. S. *J. Phys. Chem. B* **1999**, *103*, 4132.
(10) Krawiec, W.; Scanlon, L. G., Jr.; Fellner, J. P.; Vaia, R. A.; Vasudevan, S.; Giannelis, E. P. *J. Power Sources* **1995**, *54*, 310.
(11) Wieczorek, W.; Stevens, J. R.; Florjańczyk, Z. *Solid State Ionics* **1996**, *85*, 67.
(12) Kumar, B.; Scanlon, L.; Marsh, R.; Mason, R.; Higgins, R.; Baldwin, R. *Electrochim. Acta* **2001**, *46*, 1515.
(13) Croce, F.; Appetecchi, G. B.; Persi, L.; Scrosati, B. *Nature (London)* **1998**, *394*, 456.
(14) Ulrich, R.; Zwanziger, J. W.; De Paul, S. M.; Reiche, A.; Leuninger, H.; Spiess, H. W.; Wiesner, U. *Adv. Mater.* **2002**, *14*, 1134.
(15) Matyjaszewski, K., Ed. *Controlled/Living Radical Polymerization. Progress in ATRP, NMP, and RAFT*; American Chemical Society: Washington, DC, 2000.
(16) Matyjaszewski, K.; Xia, J. *Chem. Rev.* **2001**, *101*, 2921.
(17) Pyun, J.; Matyjaszewski, K.; Kowalewski, T.; Savin, D.; Patterson, G.; Kickelbick, G.; Huesing, N. *J. Am. Chem. Soc.* **2001**, *123*, 9445.
(18) Von Werne, T.; Patten, T. E. *J. Am. Chem. Soc.* **2001**, *123*, 7497.
(19) Von Werne, T.; Patten, T. E. *J. Am. Chem. Soc.* **1999**, *121*, 7409.
(20) Zhao, B.; Brittain, W. J. *J. Am. Chem. Soc.* **1999**, *121*, 3557.
(21) Szostak, R. *Molecular Sieves: Principles of Synthesis and Identification*; Van Nostrand Reinhold: New York, 1989.
(22) Krogh Andersen, E.; Krogh Andersen, I. G.; Metcalf-Johansen, J.; Simonsen, K. E.; Skou, E. *Solid State Ionics* **1988**, *28−30*, 249.
(23) Kelemen, G.; Schoen, G. *J. Mater. Sci.* **1992**, *27*, 6036.
(24) Nischwitz, P.; Amels, P.; Fetting, F. *Solid State Ionics* **1994**, *73*, 105.
(25) Feuerstein, M.; Lobo, R. F. *Solid State Ionics* **1999**, *118*, 135.
(26) Park, S.-H.; Parise, J. B.; Gies, H.; Liu, H,; Grey, C. P.; Toby, B. H. *J. Am. Chem. Soc.* **2000**, *122*, 11023.
(27) Zhan, B.-Z.; White, M. A.; Robertson, K. N.; Cameron, T. S.; Gharghouri, M. *Chem. Commun.* **2001**, 1176.
(28) Zhan, B.-Z.; White, M. A.; Lumsden, M.; Mueller-Neuhaus, J.; Robertson, K. N.; Cameron, T. S.; Gharghouri, M. *Chem. Mater.* **2002**, *14*, 3636.
(29) Zhan, B.-Z.; White, M. A.; Sham, T.-K.; Pincock, J. A.; Doucet, R. J.; Rao, K. V. R.; Robertson, K. N.; Cameron, T. S. *J. Am. Chem. Soc.* **2003**, *125*, 2195.
(30) Zhan, B.-Z.; White, M. A.; Lumsden, M.; Robertson, K. N.; Cameron, T. S. *Langmuir* **2003**, *19*, 4205.
(31) Van Oort, M. J. M.; White, M. A. *Ber. Bunsen-Ges. Phys. Chem.* **1998**, *92*, 168.
(32) Nakamoto, K. *Infrared and Raman Spectra of Inorganic and Coordination Compounds, Part A: Theory and Application in Inorganic Chemistry*, 5th ed.; John Wiley & Sons: New York, 1997.
(33) Haddleton, D. M.; Perrier, S.; Bon, S. A. F.; Waterson, C.; Irvine, D. In *Abstract Paper 219*; American Chemical Society: Washington, DC, 2000; Poly-265.
(34) Zhan, B.-Z.; Li, X.-Y. *Stud. Surf. Sci. Catal.* **1997**, *105*, 615.
(35) Zhan, B.-Z.; Li, X.-Y. *Chem. Commun.* **1998**, 349.
(36) Twu, J.; Dutta, P. K.; Kresge, C. T. *Zeolites* **1991**, *11*, 672.

MA035062Z